Editors' Suggestion

Spin glass effects and nonexistence of a ferromagnetic quantum critical point in the compositionally tuned $FeGa_{3-x}Ge_x$ metallic quantum ferromagnets ($x = 0.0 - 0.16$)

Stanislav Vrtnik,[1,2] Primož Koželj,[1,2] Magdalena Wencka,[1,3] Kristian Bader,[4] Julia Petrović,[1] Jože Luzar,[1] Peter Mihor,[1] Andreja Jelen,[1] Peter Gille,[4] and Janez Dolinšek[1,2,*]

[1]*Jožef Stefan Institute, Jamova 39, SI-1000 Ljubljana, Slovenia*

[2]*Faculty of Mathematics and Physics, University of Ljubljana, Jadranska 19, SI-1000 Ljubljana, Slovenia*

[3]*Institute of Molecular Physics, Polish Academy of Sciences, Smoluchowskiego 17, PL-60-179 Poznań, Poland*

[4]*Department of Earth and Environmental Sciences, Crystallography Section, Ludwig-Maximilians-Universität München, Theresienstrasse 41, D-80333 München, Germany*

(Received 22 April 2025; revised 25 August 2025; accepted 27 August 2025; published 11 September 2025)

Searching for a ferromagnetic (FM) quantum critical point of a compositionally tuned system, we have investigated experimentally the quantum phase transition (QPT) in the $FeGa_{3-x}Ge_x$ ($x = 0.0 - 0.16$) metallic quantum ferromagnet, by using crystallographically oriented single-crystalline samples with the Ge contents x below and within the quantum critical regime. Performing the measurements of dc and ac magnetic susceptibility and $M(H)$ curves down to the temperature of 0.4 K in low magnetic fields 0.01–25 mT, and the measurements of electrical resistivity and specific heat down to 0.35 K, we found that there is no direct, continuous transition from the paramagnetic to the FM state and consequently no FM quantum critical point in the compositional phase diagram, but the QPT involves an intermediate canonical spin glass (SG) state at $x \approx 0.12$–0.16. The compositional region of the SG state is narrow, it is formed at low temperatures (the spin freezing temperatures are in the range 1.1–1.8 K) and the coupling between the spins is weak, so that the SG ordering is fragile with respect to the external magnetic field. The analysis of the ac susceptibility via the Cole-Cole diagrams in the QPT region has revealed that the slowing-down spin dynamics of the SG state remains thermally activated down to the lowest investigated temperature of 0.4 K, so that the regime of quantum fluctuations is not yet entered. The employed experimental conditions have enabled us to follow the formation of fragile magnetic ordering in the $FeGa_{3-x}Ge_x$ compositionally tuned system in its infancy state.

DOI: 10.1103/8dh8-91qh

I. INTRODUCTION

A quantum critical point (QCP) is a point in the phase diagram of a material where a continuous (second-order) quantum phase transition (QPT) from a disordered to an ordered state takes place at absolute zero temperature, driven by a nonthermal control parameter such as pressure, magnetic field or chemical composition tuning [1–5]. The antiferromagnetic (AFM) QCP is a well-established concept [1,2,6–9], while the case of a ferromagnetic (FM) QCP is less understood. The QPTs in metallic quantum ferromagnets were reviewed by Brando *et al.* [10], distinguishing four categories of systems: (1) "clean" (mostly stoichiometric) systems that display a discontinuous (first-order) QPT from a paramagnetic to a homogeneous FM state, showing no QCP but exhibit a tricritical point in the phase diagram and the associated tricritical wings in an external magnetic field; (2) systems (mostly composition tuned, containing various degrees of disorder from weak to strong) that display a continuous QPT from the paramagnetic to a homogeneous FM state and exhibit (or are suspected to) a FM QCP; (3) systems that undergo first a phase transition to a different type of magnetic order (such as spin-density-wave or AFM) before the FM QPT is reached; and (4) strongly disordered systems (composition tuned), where the continuous FM QPT may be accompanied by short-range magnetic order, quantum Griffiths effects and spin-glass (SG) behavior in the region of the phase transition, so that precise location of the QPT is not known. Out of these four categories, only the systems from the category (2) are candidates for a FM QCP. However, since the majority of the category (2) systems are composition tuned, they contain disorder from weak to strong and a question arises whether they are really different from the category (4), because a narrow, low-temperature intermediate SG-type phase between the paramagnetic and the homogeneous FM states can easily be missed experimentally.

To elucidate this question, we have performed a study of the compositionally tuned metallic ferromagnet $FeGa_{3-x}Ge_x$ ($x = 0.0 - 0.16$) that was considered in literature a candidate for a FM quantum critical behavior at the critical Ge content

*Contact author. jani.dolinsek@ijs.si

$x_c \approx 0.15$ [11–13]. At higher x, this system becomes FM, with $T_C \approx 53$ K for $x \approx 0.27$ [14] and $T_C \approx 75$ K for $x \approx 0.41$ [15]. In the $FeGa_{3-x}Ge_x$ system, the nonmagnetic element Ga is randomly substituted by another nonmagnetic element Ge, while the concentration of the Fe remains unchanged during the substitution. The practically identical atomic radii of the Ga and Ge elements (1.24 Å of Ga versus 1.23 Å of Ge, as compared to 1.24 Å of Fe [16]) suggest minimal topological lattice distortion upon substitution. Some random structural disorder may be introduced by the moderately different Pauling electronegativities of the Ga and Ge elements (1.81 of Ga versus 2.01 of Ge, as compared to 1.83 of Fe), which locally alter the interatomic distances and bond angles. This effect could be at the origin of the reported $FeGa_{3-x}Ge_x$ tetragonal unit-cell continuous volume shrinking with increasing x, amounting to 0.3% on changing the Ge content from $x = 0.0$ to 0.33 [17]. Apart from creating the disorder, the Ge-for-Ga substitution also gives rise to electron doping of the substituted compounds (Ge has one electron more than Ga), altering their electronic properties by increasing the electron concentration in the conduction band and the associated electron density of states (DOS) at the Fermi level ε_F. Consequently, while pure $FeGa_3$ is a narrow-band semiconductor with a band gap $E_g \approx 0.3$–0.5 eV [18–20], the $FeGa_{3-x}Ge_x$ doped series is metallic, where the metallicity increases with x.

II. EXPERIMENTAL RESULTS

The magnetic, electrical, and specific heat experiments were performed on the $FeGa_{3-x}Ge_x$ oriented single crystals with the Ge contents $x = 0.0$, 0.06, 0.12, 0.14, and 0.16 (hence concentrating on the QPT region), grown by the Czochralski technique. The growth procedure, together with the XRD and chemical characterization of the materials is presented elsewhere [17]. The narrow XRD reflections reveal excellent crystallinity in the tetragonal space group $P4_2/mnm$. The cm-sized single crystals were pulled along the [001] tetragonal direction, with a small gradient of the Ge concentration along the pulling direction. For each of the above listed Ge contents x, a cubic sample of $1 \times 1 \times 1$ mm^3 dimensions was cut out for magnetic measurements, with the cube axes along the [100], [010] (both within the tetragonal plane), and [001] (the tetragonal axis) directions. In this way, the experiments could be performed along well-defined crystallographic directions on the same sample by just rotating it (and having always the same demagnetization effect, due to the cubic shape). Since the tetragonal plane is isotropic regarding the physical properties, the experiments were performed along the [100] and [001] directions, to check for the anisotropy. The volumes of the samples were small enough that the Ge content x in each sample was precise to within $\Delta x = 0.01$. As the QPTs take place at $T \to 0$, the magnetic experiments were performed down to 0.4 K. Since the possible intermediate magnetic states in the region of the QPT can be fragile with respect to the external magnetic field, we have employed a series of low magnetic fields in the range $\mu_0 H = 0.01$–25 mT (equivalent to 0.1–250 G, in cgs units) in addition to high fields up to 7 T, by nulling the residual magnetic field of the superconducting magnet to about 1×10^{-3} mT (0.01 G).

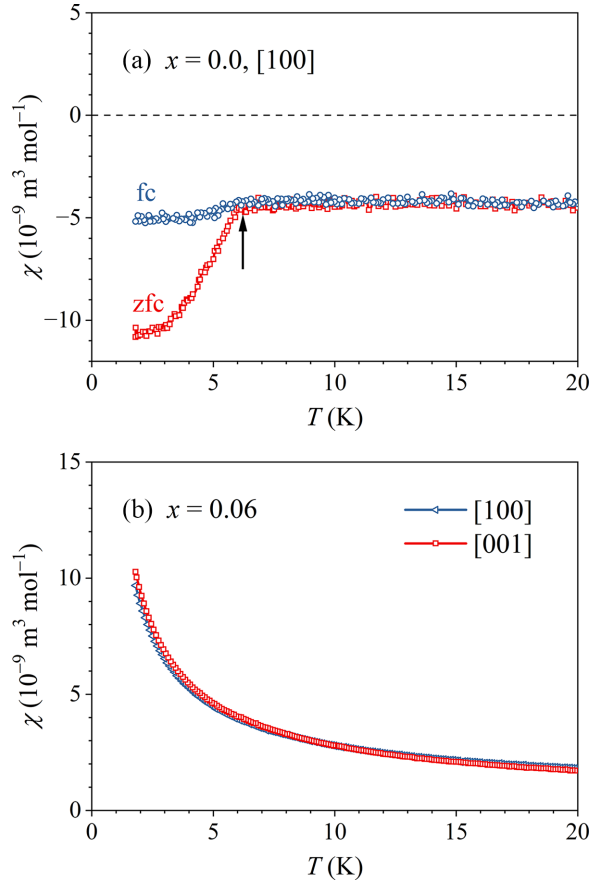

FIG. 1. (a) Zfc and fc dc susceptibilities of the $x = 0.0$ pure compound at temperatures below 20 K in a magnetic field $\mu_0 \boldsymbol{H} = 0.05$ mT applied along the [100] direction. The arrow marks the temperature where tiny amounts of Ga inclusions in thin film form get superconducting. (b) Dc susceptibilities of the $x = 0.06$ compound in a magnetic field $\mu_0 \boldsymbol{H} = 0.5$ mT at temperatures below 20 K for the field along [001] and [100] (for each direction, there is no difference between the zfc and fc susceptibilities).

A. Magnetic measurements

Direct-current (dc) magnetic susceptibility $\chi = M/H$ measurements were performed for both zero-field-cooled (zfc) and field-cooled (fc) protocols. The zfc and fc susceptibilities χ_{zfc} and χ_{fc} of the $x = 0.0$ pure compound at temperatures below 20 K in the magnetic field $\mu_0 H = 0.05$ mT applied along the [100] direction are shown in Fig. 1(a) (the results for the [001] direction are identical). χ_{zfc} and χ_{fc} are both negative diamagnetic, equal in magnitude and temperature independent down to about 6 K, amounting to -5×10^{-9} m^3 mol^{-1}. For comparison, the Larmor diamagnetic core susceptibility of the $FeGa_3$, calculated from literature tables [21] is $\chi_{\text{Larmor}} \approx -4 \times 10^{-10}$ m^3 mol^{-1}, which is of comparable magnitude. Below 6 K, a $\chi_{zfc} - \chi_{fc}$ splitting is observed, where identical splitting was already reported before for the $FeGa_3$ Czochralski monocrystal of the same origin and was identified as the Meissner effect, where tiny amounts of Ga inclusions in thin film form get superconducting below $T_C = 7.6$ K [22]. By neglecting the superconducting inclusions extrinsic to the $FeGa_3$ phase, the $x = 0.0$ pure compound is diamagnetic, supporting

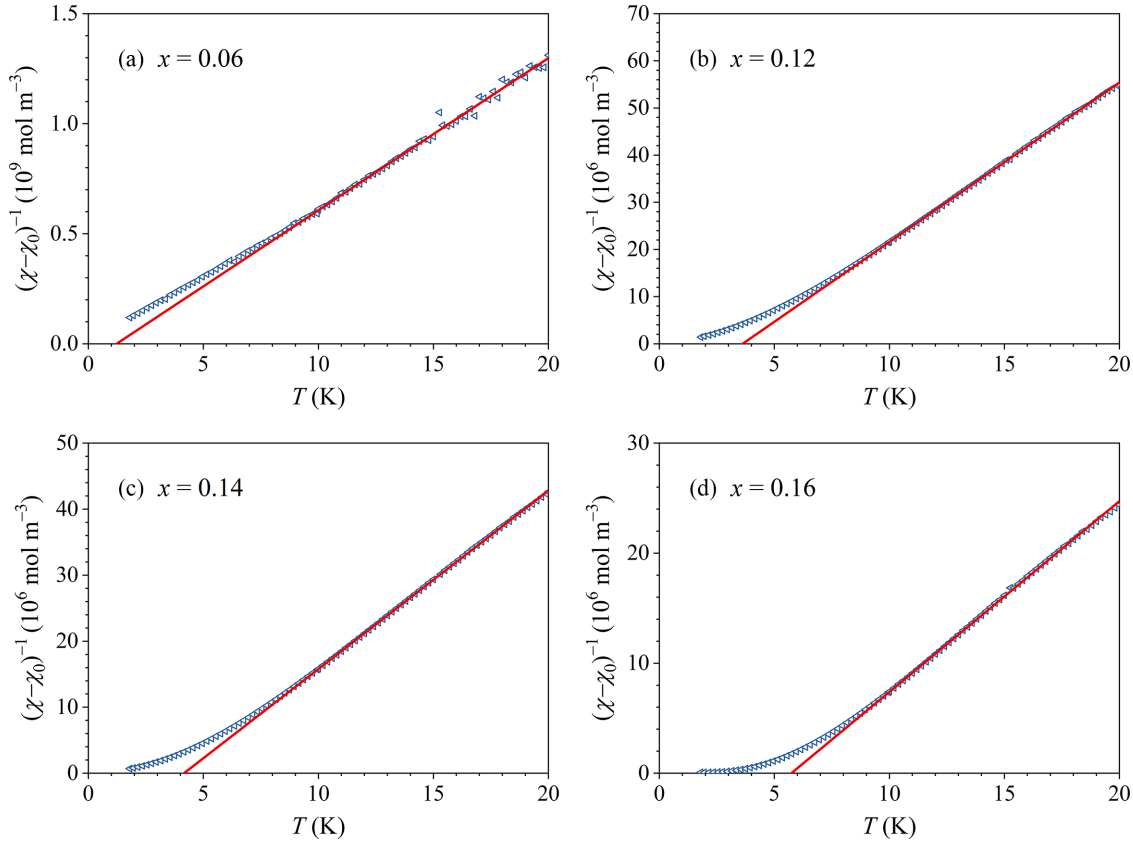

FIG. 2. Paramagnetic susceptibility (temperature range 20–1.8 K) for the field $\boldsymbol{\mu_0 H} = 0.5$ mT along [001] direction in a $(\boldsymbol{\chi} - \boldsymbol{\chi}_0)^{-1}$ vs $\boldsymbol{T}$ plot for (a) $\boldsymbol{x} = 0.06$ (b) $\boldsymbol{x} = 0.12$, (c) $\boldsymbol{x} = 0.14$, and (d) $\boldsymbol{x} = 0.16$ compounds. Solid lines are Curie-Weiss fits in the "high-temperature" range between 20 and 10 K.

the theoretical prediction that Fe in the $FeGa_3$ is nonmagnetic due to strong hybridization of the Fe $3d$ levels with the Ga $4p$ levels [18,23].

The dc susceptibilities of the $x = 0.06$ doped compound in a magnetic field $\mu_0 H = 0.5$ mT at temperatures below 20 K for the field along [001] and [100] are shown in Fig. 1(b). A Curie-Weiss type paramagnetic behavior with no noticeable anisotropy between the [001] and [100] directions is observed, demonstrating that localized magnetic moments have formed on some Fe atoms upon doping with Ge. The analysis of the susceptibility with the Curie-Weiss law $\chi = \chi_0 + C_{CW}/(T-\theta)$, where C_{CW} is the Curie-Weiss constant, θ is the Curie-Weiss temperature and χ_0 is the temperature-independent term, is presented in Fig. 2(a) in a $(\chi - \chi_0)^{-1}$ vs T plot. The fit (solid line) has yielded the effective magnetic moment (calculated from C_{CW}) $\mu_{\text{eff}} = 0.19\ \mu_B$/Fe-atom (where μ_B denotes Bohr magneton) and $\theta = 1.20 \pm 0.05$ K. The $x = 0.06$ compound remains paramagnetic down to the lowest investigated temperature of 0.4 K.

The zfc and fc dc susceptibilities of the $x = 0.12$ compound in a magnetic field $\mu_0 H = 0.02$ mT at temperatures between 15 and 0.4 K for the field along [001] and [100] direction are shown in Fig. 3(a), whereas the susceptibilities on an expanded temperature scale between 2 and 0.4 K are shown in the inset. For both field directions, the susceptibility shows the Curie-Weiss paramagnetic behavior at elevated temperatures, whereas at 1.1 K, a maximum is observed. Below the maximum, χ_{fc} and χ_{zfc} split and show different temperature dependence upon cooling. χ_{fc} tends to saturate to a temperature-independent plateau at $T \to 0$, while χ_{zfc} decreases continuously towards zero. Such behavior is typical of a spin freezing transition from the high-temperature ergodic to the low-temperature nonergodic magnetically frustrated state of a SG-type, where the onset of nonergodicity happens at the spin freezing temperature T_f, conveniently defined as the temperature of the χ_{zfc} maximum. The spin freezing transition is observed at the same temperature $T_f = 1.1$ K for both directions of the magnetic field. The marked difference between the susceptibilities for the field along [001] and [100] are their magnitudes, where the [001] susceptibility at the maximum is larger by a factor of 1.7 relative to the [100] susceptibility. This indicates that magnetocrystalline anisotropy starts to develop close to T_f, where the spins are more easily polarizable along the [001] direction than along [100] (i.e., [001] is the magnetic easy direction in the tetragonal unit cell). The susceptibility values of the $x = 0.12$ compound are by two orders of magnitude larger than those of the $x = 0.06$ compound, demonstrating that the increased Ge-for-Ga substitution has increased the fraction of magnetic Fe atoms, while the Curie-Weiss-type susceptibility confirms that the moments are localized. The Curie-Weiss analysis of the paramagnetic susceptibility in the "high-temperature" range between 20 and 10 K was performed independently for the field along [001] and [100] directions, though no dependence

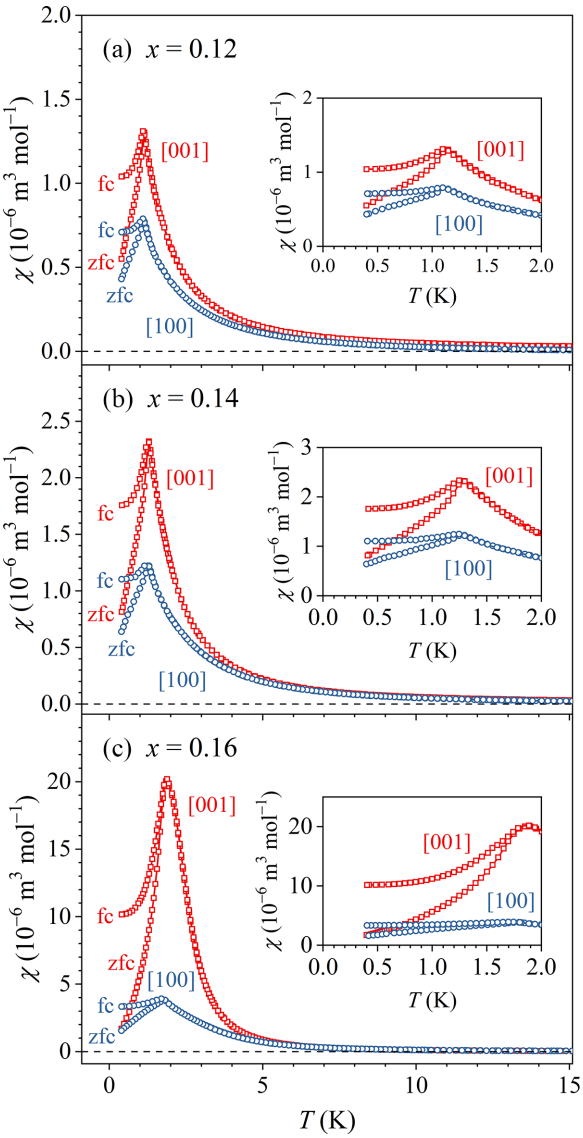

FIG. 3. Zfc and fc dc susceptibilities in a magnetic field $\boldsymbol{\mu_0 H} = 0.02$ mT at temperatures between 15 and 0.4 K for the field along [001] and [100] direction for (a) $x = 0.12$, (b) $x = 0.14$, and (c) $x = 0.16$ compounds. The susceptibilities on an expanded temperature scale between 2 and 0.4 K are shown in the insets.

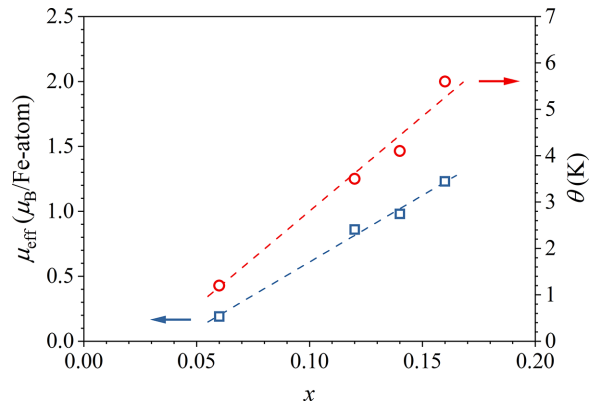

FIG. 4. The average paramagnetic moment of Fe atoms $\mu_{\rm eff}$ and the Curie-Weiss temperature θ, as a function of the Ge content x.

on the direction of the magnetic field is expected in the paramagnetic regime (as also confirmed by the analysis). The fit of the [001] zfc susceptibility in the field of 0.5 mT is shown in Fig. 2(b). The fit parameter values, averaged over the two sets of data (for the [001] and [100] field directions) are $\mu_{\rm eff} = 0.86 \pm 0.01$ μ_B/Fe-atom and $\theta = 3.5 \pm 0.1$ K.

The zfc and fc dc susceptibilities of the $x = 0.14$ [Fig. 3(b)] and $x = 0.16$ [Fig. 3(c)] compounds behave qualitatively identical to those of the $x = 0.12$ compound, showing the spin freezing transition at low temperatures and the Curie-Weiss behavior at high temperatures, with the following quantitative changes. By increasing the Ge content x, the spin freezing temperature has shifted to higher temperatures, amounting to $T_f = 1.25$ K for $x = 0.14$ and $T_f = 1.80$ K for $x = 0.16$, the magnitudes of χ_{zfc} and χ_{fc} have increased and the difference between the susceptibilities for the [001] and [100] field directions close to T_f has also increased. This indicates that upon increasing the Ge-for-Ga substitution, the fraction of magnetic Fe atoms, the strength of the interspin exchange coupling and the magnetocrystalline anisotropy all increase monotonously with the increasing Ge content x, while the Curie-Weiss-type susceptibility above T_f confirms that the Fe moments remain localized in the entire investigated substitution range up to $x = 0.16$. The Curie-Weiss analysis [Figs. 2(c) and 2(d)] has yielded $\mu_{\rm eff} = 0.98 \pm 0.01$ μ_B/Fe-atom and $\theta = 4.1 \pm 0.1$ K for the $x = 0.14$ compound and $\mu_{\rm eff} = 1.23 \pm 0.02$ μ_B/Fe-atom and $\theta = 5.6 \pm 0.1$ K for the $x = 0.16$. The graphs of $\mu_{\rm eff}$ and θ, as a function of x, are presented in Fig. 4, indicating that their increase with the Ge content is linear-like. The positive sign of θ reveals that the interspin coupling is predominantly FM-type, while the increasing θ indicates that the coupling strength increases with x. The increasing $\mu_{\rm eff}$ (the average magnetic moment of all Fe atoms in the sample) is in accord with the consideration that magnetic moments are formed on the Fe atoms located in the Ge-doped local environments.

The strength of the exchange coupling was assessed from the field dependence of the zfc and fc susceptibilities below T_f. This issue has been investigated in detail for the $x = 0.16$ compound, by performing the zfc–fc susceptibility experiments in a large set of low magnetic fields ranging from 0.01 to 25 mT. The χ_{zfc} and χ_{fc} between 2.0 and 0.4 K for the two field directions are shown in Fig. 5. Upon increasing the field, the maximum in χ_{zfc} diminishes and the $\chi_{zfc} - \chi_{fc}$ bifurcation temperature (equal to T_f in the lowest field) shifts to lower temperatures, owing to the fact that the Zeeman interaction of spins with the external magnetic field competes with the exchange interaction and tends to polarize the coupled spins into the field direction. For the [001] direction, the zfc–fc splitting is completely destroyed down to 0.4 K by the field $\mu_0 H \approx 15$ mT, whereas the [100] direction is a bit "harder" and the field of $\mu_0 H \approx 25$ mT is needed to destroy the zfc–fc splitting. This result demonstrates that the exchange interaction is weak and the internal magnetic structure that is formed below T_f in zero external field is fragile with respect to the field.

The low-temperature frustrated spin state was further characterized by the $M(H)$ magnetization versus the magnetic field curves, where the palladium standard was used to subtract the hysteresis of the superconducting magnet. We present

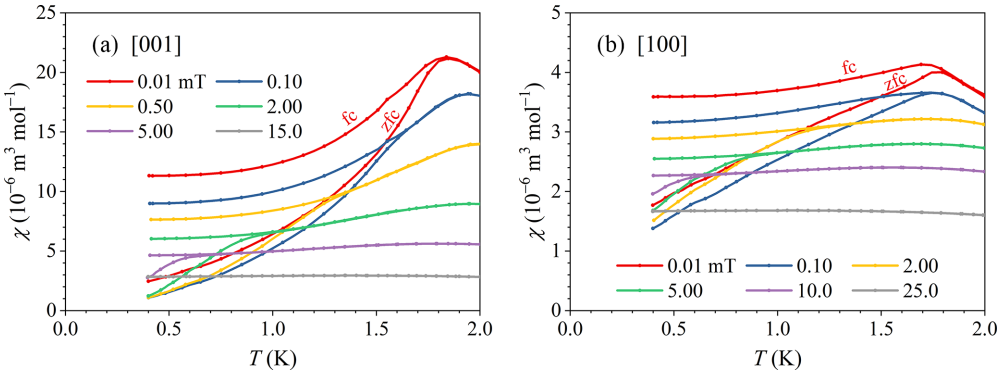

FIG. 5. Zfc and fc susceptibilities of the $x = 0.16$ compound in the temperature interval 2.0–0.4 K in magnetic fields $\mu_0 H = 0.01$–25 mT for the field along (a) [001] direction and (b) along [100].

the results for the $x = 0.16$ compound that are qualitatively valid also for the $x = 0.14$ and 0.12 compounds. The measurements were performed in the temperature interval between 2.0 and 0.4 K (recall that T_f of this compound is 1.8 K). The $M(H)$ curves at $T = 1.0$ and 0.4 K for the field sweep $\mu_0 H = \pm 0.1$ T in the fields along [001] and [100] are shown in Fig. 6, whereas the curves at $T = 0.5$ K in a larger field sweep $\mu_0 H = \pm 7$ T are shown in the inset (*i*). The curves are of a FM-type and show different approach to saturation for the two field directions, where the increase with the field is faster for the [001] direction than for the [100], confirming that [001] is the easy axis. This feature is a consequence of the single-ion magnetocrystalline anisotropy, which originates from the combined effect of the crystal-field interaction and spin-orbit coupling [24]. The second feature is the tiny hysteresis of the $M(H)$ curves in the close vicinity of $H = 0$. The hysteresis appears below 2 K (close to T_f) and increases upon cooling, being a bit larger for the [001] field direction as compared to [100]. The tiny coercive field at $T = 0.4$ K for the [001] direction amounts to $\mu_0 H_c = 2.8$ mT, while for the [100] direction it is $\mu_0 H_c = 2.0$ mT. The temperature dependence

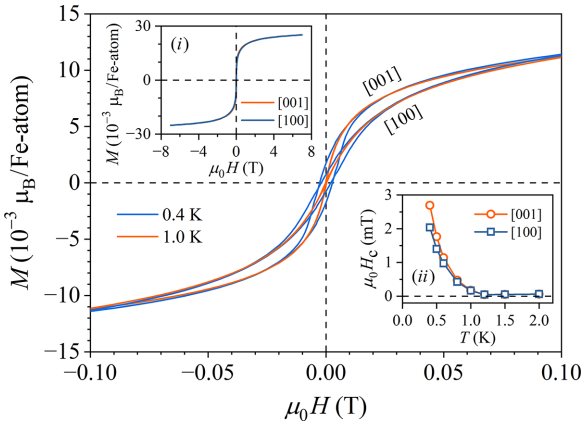

FIG. 6. $M(H)$ curves of the $x = 0.16$ compound at $T = 1.0$ and 0.4 K for the field sweep $\mu_0 H = \pm 0.1$ T applied along the [001] and [100] directions. The curves at $T = 0.5$ K in a larger field sweep $\mu_0 H = \pm 7$ T are shown in the inset (*i*) (on this scale, the curves for the two field directions are indistinguishable). The inset (*ii*) shows the coercive field H_c as a function of temperature for the two field directions.

of the coercive field is presented in the inset (*ii*) of Fig. 6. The hysteresis loops close up in a small field of $\mu_0 H \approx 30$ mT. The $M(H)$ hysteresis is a consequence of the two-ion magnetocrystalline anisotropy [24], which originates predominantly from the random distribution of exchange interactions in the magnetically frustrated state. The small value of the coercive field as well as the small close-up field reflect weakness of the exchange interaction.

Dynamic aspects (time-dependent spin fluctuations) of the low-temperature magnetically frustrated state were investigated by the alternating-current (ac) complex magnetic susceptibility $\chi(\omega) = \chi'(\omega) - i\chi''(\omega)$ in a sinusoidal magnetic field $H_{ac} = H_0 \cos \omega t$. Here $\chi'(\omega)$ is the real part of the ac susceptibility (in-phase with the field), $\chi''(\omega)$ is the imaginary (out-of-phase) part and $\omega = 2\pi\nu$, with ν denoting the frequency. The analysis was performed via the Cole-Cole diagrams, where at a certain temperature, the imaginary part $\chi''(\omega)$ is plotted versus the real part $\chi'(\omega)$ for a set of frequencies, allowing reconstructing the spectrum of spin fluctuation times at that temperature. In magnetically frustrated spin systems, this spectrum is very broad, extending over many orders of magnitude on the time axis. It is much broader than the frequency observation window of the ac susceptibility technique ($\nu = 0.1$–1000 Hz for the employed SQUID magnetometer, extending over 4 orders of magnitude), so that the spin system is nonergodic on the experimental time scale and only a limited portion of the spin fluctuation spectrum is probed experimentally. The Cole-Cole analysis was already successfully applied to SGs before [25,26].

The ac susceptibility experiments were performed on the $x = 0.16$ compound ($T_f = 1.8$ K) at 18 closely spaced temperatures between 1.9 and 0.4 K (the temperature interval ΔT was in the range 0.05–0.1 K), using the ac field of amplitude $\mu_0 H_0 = 0.2$ mT applied along the [001] direction. At each temperature, about 45 frequencies were employed, allowing accurate sampling of the experimental frequency observation window. The Cole-Cole diagrams at all investigated temperatures are presented in Fig. 7(a). The Cole-Cole diagrams were analyzed by the Havriliak-Negami (HN) relaxation model [27–29], where the relaxation equation is given by

$$\chi(\omega) = \chi_\infty + (\chi_s - \chi_\infty)/[1 + (i\omega\tau_0)^\alpha]^\beta. \qquad (1)$$

Here χ_s is the susceptibility in the static limit $\omega\tau_0 \ll 1$, χ_∞ is the (adiabatic) susceptibility in the high-frequency

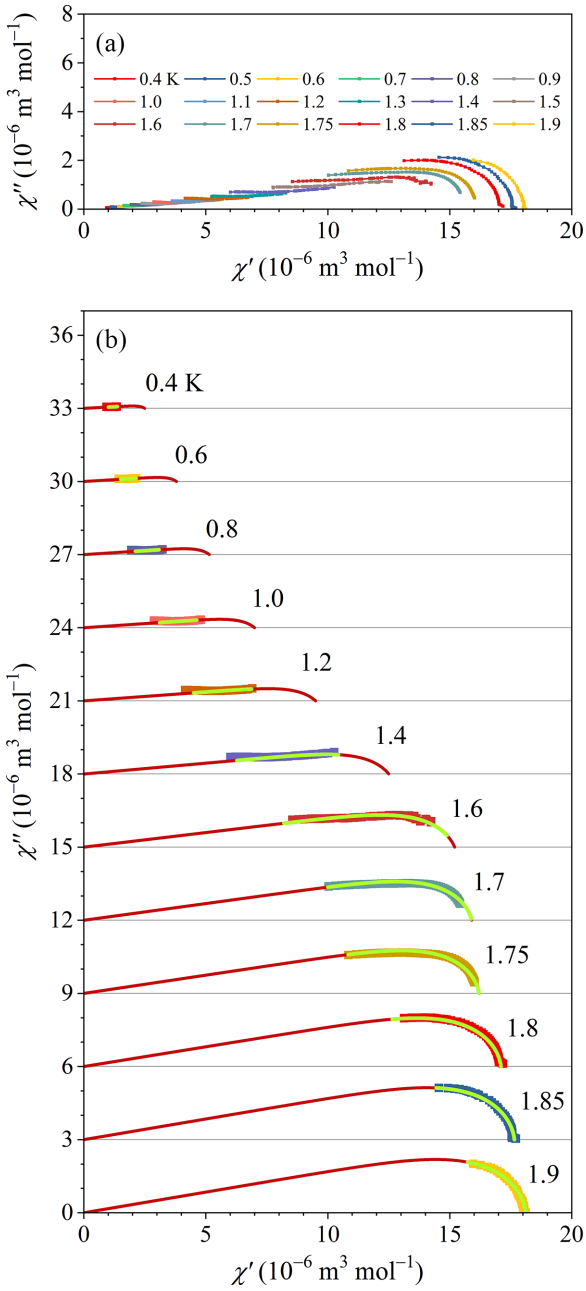

FIG. 7. (a) Ac susceptibility of the $x = 0.16$ compound (T_f = 1.8 K), presented in the form of Cole-Cole diagrams at temperatures between 1.9 and 0.4 K in an ac field of amplitude $\mu_0 H_0$ = 0.2 mT applied along the [001] direction. (b) Theoretical Cole-Cole fits of the experimental data for selected temperatures with the HN model (for clarity of presentation, the curves for each subsequent temperature are offset on the vertical axis by 3×10^{-6} m^3 mol^{-1}). The yellow-colored parts of the theoretical curves are fits of the experimental data, whereas the red parts are extrapolations into the regions outside the experimental frequency observation window. For details, see text.

limit $\omega\tau_0 \gg 1$, τ_0 is the characteristic spin fluctuation time, whereas α and β are two empirical exponents that account for the broadness and asymmetry of the fluctuation-time spectrum. The exponents assume the values on the intervals $0 < \alpha \leqslant 1$ and $0 < \beta \leqslant 1$, where the broadness and asymmetry increase on going from 1 towards 0. The expressions for $\chi'(\omega)$ and $\chi''(\omega)$ in the HN model are given in the Appendix A [Eqs. (A1)–(A3)]. The HN model is an empirical modification of the Debye relaxation model of noninteracting dipoles with a single fluctuation time τ to systems of coupled dipoles with a broad distribution of fluctuation times [30]. The Debye model is recovered from the HN model in the $\alpha = 1$ and $\beta = 1$ limit. The logarithmic distribution of spin fluctuation times $f(ln\tau)$ (the spectrum) is known analytically in the HN model [28,29], by considering that the HN relaxation can be expressed as a superposition of individual Debye relaxations

$$\frac{\chi(\omega) - \chi_\infty}{\chi_s - \chi_\infty} = \int_{-\infty}^{\infty} \frac{1}{1 + i\omega\tau} f(ln\tau)\, dln\tau, \tag{2}$$

with the real valued distribution function

$$f(ln\tau) = \frac{1}{\pi} \cdot \frac{(\tau/\tau_0)^{\alpha\beta}\sin(\beta\theta)}{[(\tau/\tau_0)^{2\alpha} + 2(\tau/\tau_0)^{\alpha}\cos(\pi\alpha) + 1]^{\beta/2}}. \tag{3}$$

The definition of the angle θ in Eq. (3) is given by Eqs. (A4)–(A5) of the Appendix A.

The analysis of the Cole-Cole diagrams was performed by fitting the experimental $\chi'(\omega)$ and $\chi''(\omega)$ data with the theoretical HN expressions given by Eqs. (A1) and (A2). Due to the nonergodicity of the spin system, i.e., the fact that the experimental frequency observation window is much narrower than the fluctuation-time spectrum, the experimental data in the Cole-Cole plots on the χ' axis do not extend over the entire range from χ_s to χ_∞, but are limited to the portion defined by the experimental window ν = 0.1–1000 Hz. The interval of the experimental data on the χ' axis is predominantly determined by the value of the τ_0 parameter and, to a lesser extent, by the values of the α and β parameters that determine the shape and width of the $f(ln\tau)$ distribution. The parameter χ_s (the static susceptibility) was in fact not a free fit parameter. For the temperatures from 1.9 to 1.7 K, its value could be read directly on the χ' axis as the point where the experimental Cole-Cole data intercept that axis, whereas at lower temperatures, the starting value was taken from the zfc static susceptibility in the 0.2 mT field presented graphically in the Appendix B and then minor adjustment was made to match the experimental amplitude of the Cole-Cole curve. The highly asymmetric shape of the Cole-Cole experimental curves at temperatures from 1.9 to 1.7 K signals strongly asymmetric $f(ln\tau)$ distribution, compatible with the β exponent deviating significantly from the symmetric case $\beta = 1$. It turned out that $\beta \approx 0.11$ was an appropriate starting fit value at the highest temperature of 1.9 K and the asymmetry has increased (β has decreased) upon cooling. The parameter α that additionally broadens the $f(ln\tau)$ distribution in a symmetric manner was unimportant at temperatures around T_f (its value between 1.9 and 1.8 K was close to 1), whereas at lower temperatures, it provided significant additional broadening of the distribution.

The theoretical Cole-Cole fits of the experimental data for a selected set of temperatures are shown in Fig. 7(b). The yellow-colored parts of the theoretical curves are fits of the experimental data, whereas the red parts are extrapolations into the regions outside the experimental frequency observation window. In determining the values of the temperature-dependent fit parameters, it was advantageous to have the

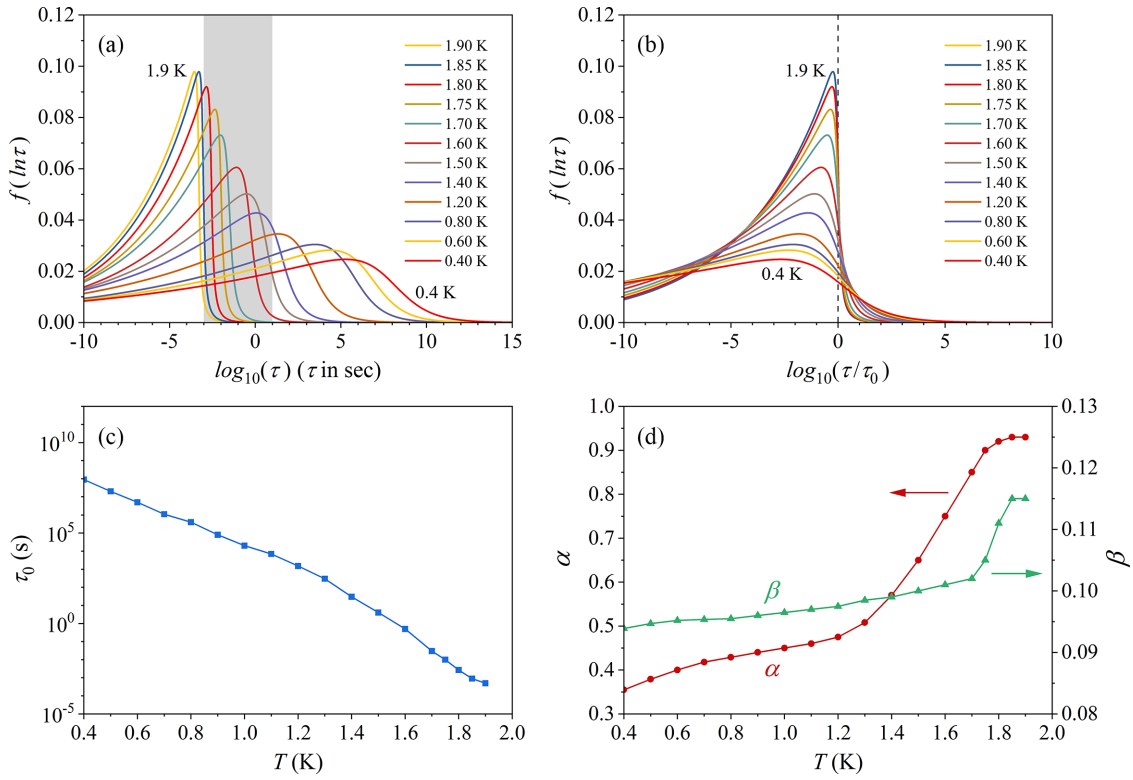

FIG. 8. (a) The distribution function $f(ln\tau)$ in the investigated temperature range 1.9–0.4 K for the $x = 0.16$ compound. The experimental time observation window (1 ms − 10 s) is gray-shaded. (b) The same distributions on the normalized scale $ln(\tau/\tau_0)$. (c) The characteristic spin fluctuation time τ_0 vs temperature (note that the vertical scale is logarithmic). (d) Temperature-dependent parameters α and β that determined the shape and width of the distribution function.

experimental data available at so many very closely spaced temperatures, so that the parameter values determined at one temperature could serve as reliable starting values for the fit at the next lower temperature and only small adjustments were needed. The fits can be considered as very good and the resulting distribution function $f(ln\tau)$ in the investigated temperature range is shown in Fig. 8(a), where the experimental time observation window (1 ms–10 s) is gray-shaded. The $f(ln\tau)$ distribution is asymmetric, with the majority of the intensity being located on the side of short fluctuation times. Close to $T_f = 1.8$ K, the distribution was estimated to extend roughly over about 12 orders of magnitude, with a rather sudden cutoff on the side of long fluctuation times at approximately 1 ms. Upon cooling, the distribution broadens and diminishes in amplitude (all distributions are normalized to the same area under the curve), and shifts continuously towards longer fluctuation times, as expected for a slowing-down spin dynamics of a magnetically frustrated state. At the lowest investigated temperature of 0.4 K, the $f(ln\tau)$ distribution spans over about 25 orders of magnitude, with the extrapolated longest fluctuation times of the order 10^8 s, equivalent to a couple of years. The same distributions on the normalized scale $ln(\tau/\tau_0)$ are shown in Fig. 8(b). The characteristic spin fluctuation time τ_0 vs temperature is shown in Fig. 8(c). With τ_0 presented on a logarithmic time scale, a linear-like continuous increase upon cooling from about 10^{-3} s at 1.9 K to 10^8 s at 0.4 K is observed. Translating this result into the direct (linear) time scale, the increase of τ_0 upon cooling is exponential, compatible with the thermally activated origin of spin fluctuations down to the lowest investigated temperature of 0.4 K. The graphs of the temperature-dependent fit parameters α and β are presented in Fig. 8(d). In the investigated temperature interval 1.9–0.4 K, β drops continuously from about 0.115 to 0.095, while α drops from 0.95 to 0.35. The χ_∞ parameter was taken as zero in the entire fitting range, where the physical significance of this choice is the assumption that in the nonergodic phase below T_f, there exist no free spins anymore in the collective SG state that could follow adiabatically the external ac field to high frequencies. The parameter χ_s was not a completely free fit parameter (as already discussed above). Its temperature dependence, together with the experimental static zfc susceptibility in the 0.2 mT field is presented graphically in the Appendix B, where reasonable matching of the two quantities is evident.

B. Electrical resistivity

Electrical resistivity was determined on rectangular-bar shaped samples of 10 mm length and 1.5 mm^2 cross section. Due to the Ge concentration gradient along the [001] direction of the Czochralski ingot, the bars were cut with the long dimension along the [100] direction that is perpendicular to the gradient direction, in order to have a sharply defined Ge content x. [100] was also the direction of the electrical current. The resistivity ρ of the $x = 0.0$ pure compound in the temperature range 300–1.8 K is shown in Fig. 9(a). The resistivity is typical of a semiconductor with in-gap states (a

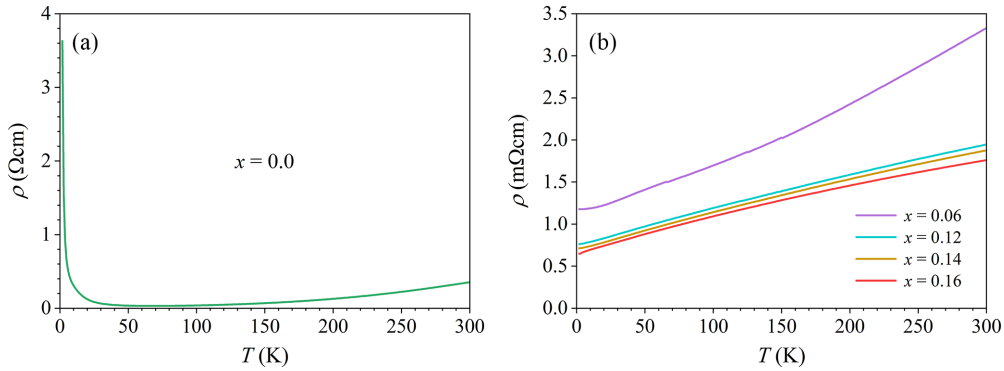

FIG. 9. (a) Electrical resistivity of the $x = 0.0$ pure compound in the temperature range 300–1.8 K. (b) The resistivities of the doped compounds $x = 0.06 - 0.16$ in the interval 300–1.8 K.

doped-type semiconductor), showing a large low-temperature resistivity $\rho_{1.8K} \approx 3600$ mΩcm and a rapid decrease upon heating to $\rho_{60K} = 32$ mΩcm, due to thermal excitation of the electrons from the in-gap states into the conduction band. This rapid drop is followed by a moderate increase of the resistivity towards the room temperature, amounting to $\rho_{300K} = 350$ mΩcm. This resistivity is identical to the one reported before for the $FeGa_3$ Czochralski monocrystal of the same origin [22] (studied there to the temperature of 950 K).

The resistivities of the doped compounds $x = 0.06 - 0.16$ in the interval 300–1.8 K are shown in Fig. 9(b). Doping with Ge has significantly decreased the resistivity and changed it into a metallic type with a positive temperature coefficient. The decrease is directly correlated to the amount of Ge doping x, where the resistivity of the $x = 0.06$ compound is the highest and the $x = 0.16$ resistivity is the lowest. The $T \to 0$ values are in the range $\rho_{1.8K} = 0.7$–1.2 mΩcm and room temperature values are in the range $\rho_{300K} = 1.8$–3.4 mΩcm. These resistivity values, though 2 to 3 orders of magnitude smaller than the one of the $x = 0.0$ pure (semiconducting) compound, are still high as compared to regular metals and alloys, where the values in the range $\rho \approx 1$–100 μΩcm are typical. This suggests that the charge carrier concentration in the conduction band is reduced in comparison to regular metals, i.e., the $FeGa_{3-x}Ge_x$ doped compounds exhibit weakly metallic character and their metallicity increases with x.

C. Specific heat

The low-temperature state of the $FeGa_{3-x}Ge_x$ compounds was further characterized by the specific heat experiments, considering that the total specific heat is a sum $C = C_{el} + C_{\text{latt}} + C_{\text{mag}}$. The term $C_{el} = \gamma T$ is the electronic contribution that is linear in temperature up to the melting point and $\gamma = (\pi^2/3)k_B^2 g(\varepsilon_F)$ is the electronic specific heat coefficient, where $g(\varepsilon_F)$ is the electron DOS at ε_F. C_{latt} is the lattice (phononic) contribution, which can be at temperatures below about 10 K written in the Debye approximation as $C_{\text{latt}} = \beta T^3$, with $\beta = 12\pi^4 R/5\theta_D^3$, where θ_D is the Debye temperature and R is the gas constant. At slightly elevated temperatures, higher-order corrections are usually employed, where the leading term is $\beta_5 T^5$. The term C_{mag} is the magnetic specific heat, representing the heat released from the spin system due to lowering of its exchange energy by spin ordering.

The specific heat measurements were performed on cubic-shaped samples of 1 mm^3 volume in the temperature range 300–0.35 K in zero magnetic field (in order not to disturb the fragile spin structure that forms at low temperatures in the absence of the field). The low-temperature total specific heat C of all samples at temperatures between 17 and 0.35 K is shown in Fig. 10(a) in a C/T vs T^2 plot. If there were no C_{mag} contribution, the specific heat curves $C/T = \gamma + \beta T^2$ would be straight lines in this kind of a plot, with the $T = 0$ intercept on the vertical axis given by the electronic coefficient γ and the slope determined by the lattice coefficient β. In Fig. 10(a) it is observed that the specific heat curves away from the $T \to 0$ limit are indeed linear-like lines with almost the same slopes, and the curves are systematically shifted vertically with the increasing Ge content x. The vertical shifts signal the increase of γ (and the associated DOS at ε_F value) with x due to the increased metallicity of the $FeGa_{3-x}Ge_x$ compounds, while the almost identical slopes indicate that the lattice specific heat is about the same for all of them. The latter result reflects the fact that all compounds share a common crystal structure and the tetragonal unit cell parameters a and c change very little with the increased Ge concentration, which makes their phonon spectra very similar. In the $T \to 0$ limit, the C/T curves of the doped compounds show an upturn, the magnitude of which increases with x. This upturn was attributed to the magnetic specific heat C_{mag}.

In order to determine the values of γ and β of each compound and to extract the magnetic contribution C_{mag}, the following strategy was employed. According to the Curie-Weiss analysis of the magnetic susceptibility presented in Fig. 2, the departure from the Curie-Weiss behavior of the doped compounds due to the formation of magnetic short-range order happens below about 9 K, so that above that temperature it is reasonable to assume that $C_{\text{mag}} = 0$. The total specific heat in the temperature interval 9–14 K was consequently fitted with the expression $C = \gamma T + \beta T^3 + \beta_5 T^5$ and the coefficients γ, β and β_5 were determined. The validity of this procedure was tested on the $x = 0.0$ pure compound that has no magnetic contribution ($C_{\text{mag}} = 0$), where the analysis has yielded the values $\gamma = 0.036$ $mJmol^{-1}K^{-2}$, $\beta = 0.04$ $mJmol^{-1}K^{-4}$, and $\beta_5 = 2\times10^{-6}$ $mJmol^{-1}K^{-6}$. The so determined γ value is in good agreement with the value $\gamma = 0.03$ $mJmol^{-1}K^{-2}$, reported before for the $FeGa_3$ Czochralski monocrystal of the same origin [22], confirming that the

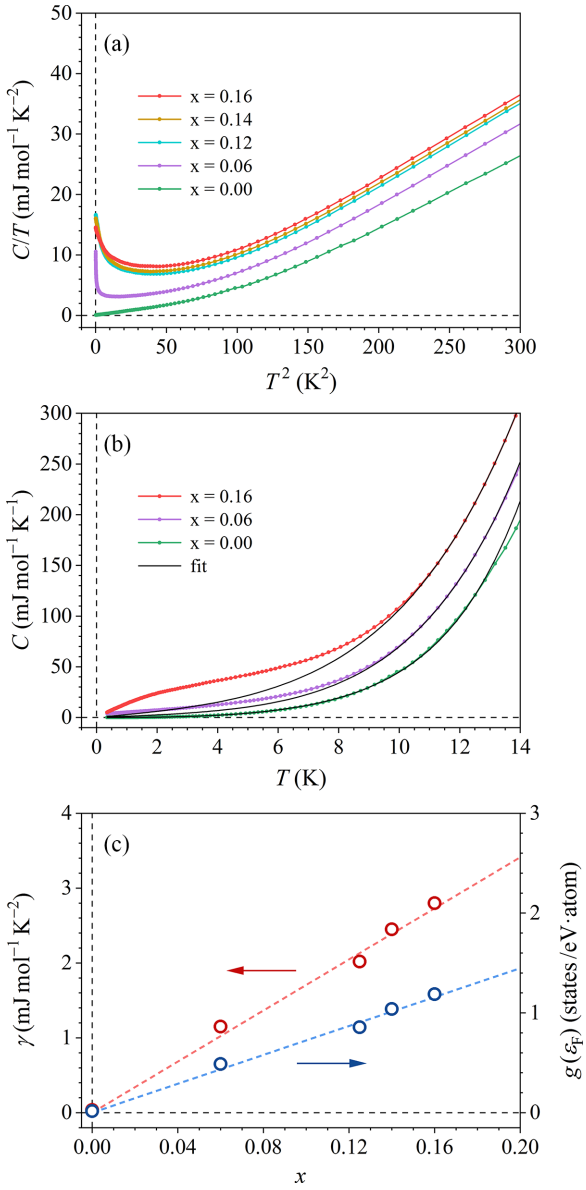

FIG. 10. (a) Low-temperature total specific heat C of all samples ($x = 0.0 - 0.16$) in zero external magnetic field at temperatures between 17 and 0.35 K in a C/T vs T^2 plot. (b) Low-temperature total specific heat of the $x = 0.0$, 0.06, and 0.16 compounds in a C vs T plot, fitted with the expression $C = \gamma T + \beta T^3 + \beta_5 T^5$ in the temperature interval 9–14 K and then extrapolated to $T \to 0$ (solid curves). (c) The electronic specific heat coefficient γ and the electron DOS at ε_F, as a function of Ge content x.

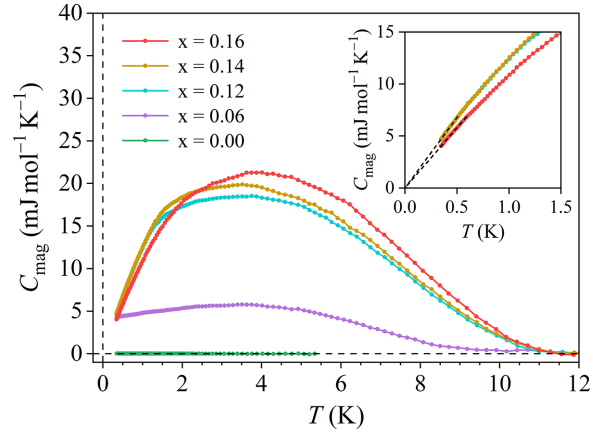

FIG. 11. Temperature-dependent magnetic specific heat C_{mag} of all samples ($x = 0.0 - 0.16$) in zero external magnetic field. The linear vanishing of C_{mag} in the $T \to 0$ limit for the three SG-type compounds $x = 0.12$, 0.14, and 0.16 is demonstrated in the inset, where the dashed lines are guides for the eye (the datasets of the $x = 0.12$ and 0.14 compounds in the inset are indistinguishable).

extrapolation of the 9–14 K fit towards $T \to 0$ gives a valid result. The Debye temperature obtained from β amounts to $\theta_D = 360 \pm 10$ K, which can be considered valid for the whole $FeGa_{3-x}Ge_x$ series. The above procedure, applied to other $FeGa_{3-x}Ge_x$ compounds [Fig. 10(b)] has yielded γ that increases linearly with x from the value 0.036 $\mathrm{mJmol^{-1}\,K^{-2}}$ for $x = 0.0$ to 2.8 $\mathrm{mJmol^{-1}\,K^{-2}}$ for $x = 0.16$ [Fig. 10(c)]. The γ values allow calculating the DOS at ε_F by using the formula $\gamma = 2.358 g(\varepsilon_F)$, where γ is inserted in units of $\mathrm{mJmol^{-1}\,K^{-2}}$ and $g(\varepsilon_F)$ is then in units states/eV·atom [31]. The $g(\varepsilon_F)$ vs x is also presented in Fig. 10(c), increasing linearly from $g(\varepsilon_F) = 0.015$ states/eV·atom for $x = 0.0$ to 1.2 states/eV·atom for $x = 0.16$.

Having determined the electronic and lattice contributions for all compounds, the C_{mag} was obtained by a subtraction procedure $C_{\mathrm{mag}} = C - \gamma T - \beta T^3 - \beta_5 T^5$ and the results are presented in Fig. 11. As expected, the magnetic specific heat of the $x = 0.0$ nonmagnetic compound is zero, while C_{mag}s of the doped compounds are nonzero and increase in magnitude with the doping x, reflecting the increased number of Fe magnetic moments. The magnetic specific heats of the three SG-type compounds $x = 0.12$, 0.14, and 0.16 show qualitatively identical temperature dependence, with the following features. Upon cooling, C_{mag} becomes nonzero at temperatures below about 10 K, passes through a broad maximum and then decreases, vanishing linearly with the temperature, $C_{\mathrm{mag}} \propto T$, in the $T \to 0$ limit (inset in Fig. 11). Such behavior is characteristic of spin glasses and other magnetically frustrated systems, where the onset of spin freezing starts below the temperature of the order of $10T_f$ due to the formation of magnetic short-range order, the peak in C_{mag} is formed at a temperature somewhat greater than T_f (for the $x = 0.16$ compound, the peak in C_{mag} occurs at about 3.5 K, whereas T_f determined from χ_{zfc} is 1.8 K), while the asymptotic behavior at $T \ll T_f$ is $C_{\mathrm{mag}} = AT$ (with A being a constant) [32]. Figure 11 reveals that the C_{mag} maximum shifts to lower temperatures for the compounds with smaller x, which is in agreement with their lower T_f values. The $x = 0.06$ compound behaves at first glance a bit different, where C_{mag} becomes nonzero below about 8 K and then increases towards $T = 0$ without a tendency of vanishing linearly in the $T \to 0$ limit, but this behavior can still be explained within the same physical picture. The magnetization measurements show that this compound remains paramagnetic down to the lowest investigated temperature of 0.4 K, whereas the departure of the susceptibility from the Curie-Weiss behavior below about 8 K demonstrates the appearance of magnetic short-range order below that temperature. The C_{mag} of the $x = 0.06$

compound is hence also of the SG-type, corresponding to the high-temperature side of the peak.

III. DISCUSSION

The presented experiments on crystallographically oriented single-crystalline $FeGa_{3-x}Ge_x$ samples with the Ge contents x below and within the quantum critical regime, performed down to low temperatures in the sub-Kelvin range and in low magnetic fields of the order 0.1 mT, have enabled us to follow the formation of fragile magnetic ordering in the $FeGa_{3-x}Ge_x$ compositionally tuned system in its infancy state. The key factors that drive this system from a nonmagnetic semiconductor at $x = 0$ through the SG-type QPT at $x = 0.12 - 0.16$ to the long-range ordered FM state at larger x by the increased Ge-for-Ga doping are (1) the appearance and increase in number of the localized Fe magnetic moments and the associated decrease of the average distance between them, (2) the increased number of conduction electrons in the conduction band (increased metallicity), and (3) the consequent increase in strength of the interspin coupling between the Fe moments. The coupling is considered to be the indirect exchange Ruderman-Kittel-Kasuya-Yosida (RKKY) interaction, and the increase of the coupling strength via doping is supported by the following physical picture. The RKKY coupling between two localized spins $\vec{S}_i$ and $\vec{S}_j$, separated by a distance r is represented by a Hamiltonian $\mathcal{H} = -\mathcal{J}(r)\vec{S}_i \cdot \vec{S}_j$, where the coupling constant at large distances is given by $\mathcal{J}(r) = \mathcal{J}_0 \cos(2k_F r)/(2k_F r)^3$. Here $\mathcal{J}_0 = \eta Z J_{sd}^2 g(\varepsilon_F)$, with Z denoting the number of conduction electrons per atom, J_{sd} is the $s-d$ exchange constant between the localized d-spin and the conduction electrons, η is a numerical constant, and k_F is the Fermi momentum [33]. The relation between the spin freezing temperature T_f of a spin glass and the RKKY coupling strength may be viewed from a simple model. By considering only the *envelope* of the RKKY oscillations, the strength of the interaction as a function of distance r is $\mathcal{J}'(r) = \mathcal{J}_0'/r^3$ (where $\mathcal{J}_0' = \mathcal{J}_0/(2k_F)^3$). Considering that the Fe moments are formed in local environments where the Ge-for-Ga substitution took place (and assuming a single-atom substitution within each Fe nearest-neighbor environment), the average distance between two magnetic moments is related to the Ge concentration c_{Ge} as $\bar{r} = (1/c_{Ge})^{1/3}$. The thermal disordering energy that destroys the correlations between spins that are $\bar{r}$ apart is $k_B T$. For the spin freezing to occur, the RKKY interaction must be greater than the thermal disordering energy, which sets the relation $\mathcal{J}'(\bar{r}) = k_B T_f$, or $T_f = c_{Ge}\mathcal{J}_0'/k_B$ [33]. Since $\mathcal{J}_0' \propto g(\varepsilon_F)$, a one-to-one correlation between T_f and the product $c_{Ge}g(\varepsilon_F)$ (or equivalently $c_{Ge}\gamma$, where γ is the electronic specific heat coefficient) is expected. The graph of T_f versus $c_{Ge}\gamma$ for the three SG-type compositions $x = 0.12$, 0.14, and 0.16 is shown in Fig. 12, where a positive, linear-like correlation is evident, supporting that the RKKY coupling strength increases with the increased Ge-for-Ga doping. Here we note that in establishing the above T_f vs $c_{Ge}\gamma$ relation, we have neglected the fact that the number of conduction electrons per atom Z appearing in $\mathcal{J}_0'$ also changes with the doping. In the narrow SG regime $x \approx 0.12$–0.16, this approximation can be justified by considering that the conduction

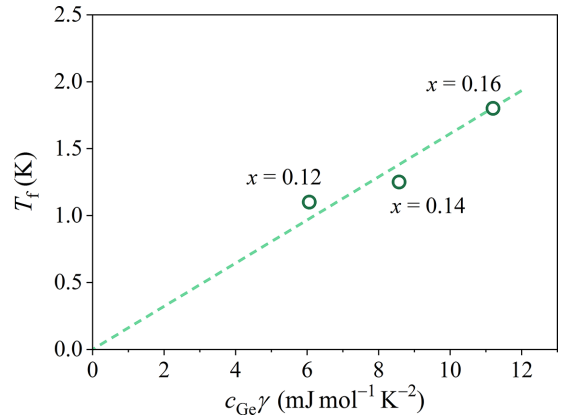

FIG. 12. Correlation between the spin freezing temperature T_f and the product $c_{Ge}\gamma$ (where c_{Ge} is the Ge concentration (taken in at.%) and γ is the electronic specific heat coefficient, proportional to the electron DOS at ε_F) for the three SG compositions $x = 0.12$, 0.14, and 0.16.

electrons originate from both Ga and Ge atoms due to the change of the electronic band structure. To this end, one needs to take into account the number of valence electrons per atom e/a by considering an "average" $Ga_{(3-x)/3}Ge_{x/3}$ atom. The electronic configuration of Ga is [Ne] $3s^2\,3p^1$, donating 3 electrons into the conduction band in a fully metallic state, while the configuration of Ge is [Ne] $3s^2\,3p^2$, donating 4 electrons. The e/a for the "pure" $x = 0$ average atom is hence 3, while it becomes 3.040, 3.047, and 3.053 for the $x = 0.12$, 0.14, and 0.16, respectively. In the metallic state of the $FeGa_{3-x}Ge_x$ doped compounds, it is reasonable to assume that $Z \propto e/a$, and small departures of e/a from the value 3 justify why it is not necessary to include Z into the T_f vs $c_{Ge}\gamma$ relation.

We discuss next the "birth" and evolution of the $FeGa_{3-x}Ge_x$ magnetic state upon doping, starting from a nonmagnetic state at $x = 0$, followed by a paramagnetic state at small x that evolves into a SG state for x in the critical region and then reaching a long-range ordered FM state at higher x. We begin with a qualitative description of the formation of magnetic moments on the Fe atoms upon the Ge-for-Ga substitution. The tetragonal unit cell of the $FeGa_3$ pure compound ($a = 626.28$ pm, $c = 655.46$ pm) contains 4 Fe and 12 Ga atoms, with the Fe atoms forming two Fe–Fe dimer pairs (Fe–Fe distance $d = 277$ pm), one along [110] direction in the $z = 0$ plane and the other along $[1\bar{1}0]$ in the $z = 1/2$ plane, while the 12 Ga atoms occupy two crystallographic sites, 4 Ga1 and 8 Ga2, so that the total composition of the unit cell is $Fe_4Ga1_4Ga2_8$ [34]. The heteroatomic coordination of each Fe atom includes 8 Ga atoms, 2 Ga1 at the distance $d_1 =$ 237 pm to Fe, 2 Ga2 ($d_2 = 239$ pm) and 4 Ga2 ($d_3 = 250$ pm). Density-functional-theory (DFT) calculations have predicted that the Ge atom is preferentially substituted for the Ga1 sites [13], so we assume that the nearest-neighbor environment of a given Fe atom can contain either zero, one, or two Ge atoms. The Fe atoms in unsubstituted environments are nonmagnetic due to the hybridization of the Fe $3d$ levels with the Ga $4p$ levels [18,23], while in the substituted environments, the Fe moments develop because the local electronic structure is changed. We further assume that the substitution of a Ge atom into a given local Fe environment promotes moment

formation only on that particular Fe atom, whereas it has no effect on other, more distant Fe atoms. The assumption is based on the DFT supercell calculations for the $x = 0.125$ composition [13], predicting theoretically that the electron density is perturbed within the range 300–400 pm (3–4 Å) from the Ge atom, affecting only the Ga sites and the Fe atom in the close vicinity of the Ge atom. This approximation can be considered valid in the low-doping regime, before the Ge concentration becomes high enough to form the FM state. In the low-doping regime, it is also reasonable to anticipate that the Ge-for-Ga substitution at the 4 Fe atoms in the unit cell is random.

At the beginning of the substitution (small x), localized Fe moments appear randomly on some Fe sites. Considering the particular case $x = 0.06$, the composition $FeGa_{2.94}Ge_{0.06}$ infers that there is one Ge atom present per 49 Ga atoms. For a single-atom substitution per unit cell, i.e., out of the four Fe nearest-neighbor environments, only one contains a single Ge atom, and since there are 12 Ga atoms in the unit cell, then every fourth unit cell would contain an Fe magnetic moment on average. The moments are hence distant and since the RKKY interaction is still very weak, the moments do not feel each other considerably and the paramagnetic state results. Upon increasing the x, the number of localized Fe moments increases, the interspin distances decrease and there can be more than one substitution per unit cell, randomly distributed over the four Fe environments. The spins are thus positioned randomly on the iron sublattice. The strength of the RKKY interaction also increases and since it oscillates with the interspin distance between positive and negative values on the scale of nanometers, some pairs of spins favor parallel (FM) and the others antiparallel (AFM) alignment, as also predicted by the DFT calculations [14]. The spin system contains mixed FM-AFM interactions, and since RKKY is a long-range interaction, the spins are subjected to competing interactions with many neighbors, which results in frustration of the collective spin state. Consequently, the system fulfills two basic requirements to be classified as a site-disordered spin glass: (*i*) randomness (the spins are positioned randomly in the lattice) and (*ii*) frustration (no spin configuration can satisfy all the bonds and minimize the free energy at the same time) [35]. In the $FeGa_{3-x}Ge_x$, this situation happens at $x \approx 0.12$–0.16, where the amount of Ge "impurities" is still not in the concentrated limit. For $x = 0.12$, the composition $FeGa_{2.88}Ge_{0.12}$ infers that there is one Ge atom present per 24 Ga atoms, so that every second unit cell contains a magnetic Fe on average, while for $x = 0.16$, there is one magnetic Fe per 1.5 unit cells.

Upon further increase of the Ge content x, the RKKY coupling strength continues to increase and the sites of the iron periodic sublattice get progressively filled with the magnetic moments, so that the distribution of moments gradually changes from random to periodic. The spin system consequently enters the concentrated limit. In the periodic case, the nature (the sign) of the RKKY interaction drives the spin system to an FM state. At the x values still not high enough that all Fe sites would develop magnetic moments, the FM state is inhomogeneous (site-disordered), while it becomes homogeneous (site-ordered) FM when all sites of the iron sublattice contain magnetic moments. Full periodicity of the magnetic lattice would be achieved for all four Fe sites within each unit cell magnetic. Assuming that only one Ga1 atom out of the possible two in each Fe local environment would be substituted by Ge (i.e., there would be 4 Ge atoms and 8 Ga in the unit cell), the homogeneous FM state could be expected at the composition $FeGa_2Ge_1$, i.e., at $x = 1.0$. This x value should not be taken literally, because in the Ge-concentrated limit, it is plausible that a Ge atom in a given Fe local environment does not affect only that particular Fe atom to develop a magnetic moment, but also other neighboring Fe atoms, so that the homogeneous FM state likely appears at lower x values already. It was reported that the $x \approx 0.27$ composition is FM with $T_C \approx 53$ K [14], but the question whether the FM state is inhomogeneous or homogeneous has not been considered. In addition, a structural phase transition from the space group $P4_2/mnm$ to a different crystal symmetry is likely to occur in the Ge-concentrated limit, where the above considerations break down. The composition $FeGa_{2.59}Ge_{0.41}$ ($x = 0.41$) still preserves the space group $P4_2/mnm$ [15], whereas there are no literature reports for higher x values.

IV. CONCLUSIONS

The above-described evolution of the magnetic state in the $FeGa_{3-x}Ge_x$ compositionally tuned system by doping shows that this is a continuous process, involving the following sequence of states: diamagnet → paramagnet → spin glass → ferromagnet. There are no sharp "critical" values of x where the changes of the magnetic state occur. A direct transition from a paramagnet to a homogeneous ferromagnet does not take place, but involves an intermediate SG state, so that there is consequently no FM QCP in the magnetic phase diagram. The region of the SG phase is narrow (Ge content in the range $x \approx 0.12$–0.16), the phase is formed at low temperatures (T_fs are between 1.1 and 1.8 K) and the coupling between the spins is weak, so that the SG ordering is fragile with respect to the external magnetic field (the fields of a few mT already destroy the internal magnetic structure). Such compositionally narrow, low-temperature, magnetically fragile SG state can easily be missed experimentally. Since tuning of the composition always introduces some degree of disorder into the spin system, the discovery of a narrow intermediate SG state in the $FeGa_{3-x}Ge_x$ raises the question of whether an intermediate SG state between the paramagnetic and the homogeneous FM states could be present also in other compositionally tuned magnetic system that were reported to undergo a continuous FM QPT in the $T \to 0$ limit? Those systems, belonging to the class (2) of Brando *et al.'s* [10] classification of QPTs in metallic quantum ferromagnets would then be essentially the same as the systems of the class (4) (composition tuned systems, where the continuous FM QPT may be accompanied by short-range magnetic order, quantum Griffiths effects, and spin-glass behavior in the region of the phase transition, so that precise location of the QPT is not known). The FM QPTs take place in a number of very different systems including d-electron and f-electron systems, metals or metallic insulators (undergoing a metal-to-insulator transition), with itinerant/localized magnetic moments, in the presence/absence of an inversion symmetry [10,36,37]. To throw some light on this fundamental question, we make

comparison of the $FeGa_{3-x}Ge_x$ system to other compositionally tuned systems reported in literature to undergo a continuous FM QPT and exhibit (or are suspected to) a QCP (the list is not exhaustive). We begin with the Ni_xPd_{1-x} system, where the FM Curie temperature of pure Ni metal $T_C \approx$ 600 K can be reduced by substituting Pd for Ni. By varying x in the range 0–0.1, the transition temperature was reduced to $T_C \approx 7$ K (the lowest achieved T_C in these experiments) and the critical concentration of the FM QCP was estimated as $x_c = 0.025$ [38]. Subsequent ac susceptibility and zfc–fc magnetization experiments on the same samples found evidence for SG freezing in a small region of the phase diagram $0.025 \leqslant x \leqslant 0.028$ [39], putting the Ni_xPd_{1-x} system on the same ground with the $FeGa_{3-x}Ge_x$. The FM order in the Ni_3Al with $T_C = 41$ K can be suppressed by substituting Pd for Ni (the $(Ni_{1-x}Pd_x)_3Al$ system [40]) or by doping with Ga (the $Ni_3Al_{1-x}Ga_x$ system [41]). The former system was investigated for the Pd content range $x =$ 0–0.20 and T_C has decreased from 41 K to the lowest measured $T_C \approx 4$ K, estimating the QCP at $x_c \approx 0.095$. In the $Ni_3Al_{1-x}Ga_x$ system, T_C was reduced from 41 to 5 K in the range $x =$ 0–0.33, with the subsequent extrapolation of the $T_C(x)$ curve predicting the QCP at $x_c \approx 0.34$. For both systems, the possible presence of a narrow SG-type phase (or some other collective phase) in the close vicinity of x_c was not reported. In the $(Cr_{1-x}Fe_x)_2B$ system, ferromagnetism can be induced by doping the paramagnetic compound Cr_2B with Fe. For x in the range 0.05–0.025, T_C has shifted from 45 to 8 K and the critical concentration of the QCP was estimated to be $x_c \approx 0.02$ [42], while the existence of a narrow SG phase in the immediate vicinity of x_c was not reported. Itinerant ferromagnetism in the $ZrZn_2$ ($T_C = 28.5$ K) can be tuned to zero by a small amount of Nb substituting for Zr (the $Zr_{1-x}Nb_xZn_2$ system). Investigating this system in the range $x =$ 0–0.14 down to the temperature 1.8 K, the Arrott-plot analysis revealed that T_C is suppressed to zero at $x_c \approx 0.083$ [43]. No indication of new collective phases near the QCP was found, but the Authors suggest that *further measurements at lower temperatures and with refined samples would be very interesting to further pursue this issue*. The $SrCo_2Ge_2$ Pauli paramagnet develops ferromagnetism by doping with P (the $SrCo_2(Ge_{1-x}P_x)_2$ system) at $x \approx 0.325$ [44]. Within the P content range $x =$ 0.55–0.35, T_C was reported to decrease from 35 to 5 K and the QCP was predicted at $x_c \approx$ 0.325. For $x > x_C$, the Curie temperature first increases with increasing x, reaches a maximum of $T_C \approx 35$ K at $x \approx 0.55$ and then decreases. No sign of a first-order transition or SG behavior was detected in those studies. URu_2Si_2, a parent compound of the $URu_{2-x}Re_xSi_2$ system, is a heavy-fermion superconductor (superconducting $T_c \approx 1.5$ K) that has an ordered phase of unknown nature, usually referred to as the "hidden-order" phase, below about 17 K [45]. Doping with Re results in disappearance of the hidden-order phase at $x \approx 0.1$ and ferromagnetism develops for $x \gtrsim 0.15$, but the critical Re concentration x_c was hard to determine [46]. For x in the range 0.6–0.2 K, T_C was reported to decrease from 25 to 2 K. The uncertainty in x_c was considered to be related to the fact that there is a Re concentration range that represents a quantum Griffiths phase rather than a true long-range FM order. This indicates the existence of an intermediate collective magnetic phase between the paramagnetic and the homogeneous FM states, though the $URu_{2-x}Re_xSi_2$ is considered a system with a second-order FM QPT. The $YbNi_4(P_{1-x}As_x)_2$ system is a quasi-one-dimensional material, where doping with As reduces the T_C. Studying this system for the composition range $x =$ 0–0.13 [37], the Curie temperatures were found to be very low, decreasing from $T_C = 150$ mK at $x = 0$ to $T_C = 25$ mK at $x = 0.08$ (the lowest T_C measured in these experiments). Extrapolating the $T_C(x)$ curve then predicted the FM QCP at $x_c \approx 0.1$. The FM QPT was reported to remain of second order even in the sample with $x = 0.08$ that was closest to x_c, ruling out the possible quantum Griffith phase at that composition. The above literature survey indicates that some studies report a narrow intermediate SG-type phase in the close vicinity of the critical composition x_c, while most studies do not. The detection of such phase(s) may require pretentious experimental conditions, by preferably employing oriented monocrystalline samples with accurate and closely spaced dopant concentrations x on both sides of x_c, low temperatures down to the sub-Kelvin range and accurate and repeatable tiny magnetic fields of the order 0.01–0.1 mT (recall that the earth's magnetic field is in the range 0.02–0.07 mT).

It should be stressed that the above considerations refer to the compositionally tuned systems only and do not question the possibility of a fully continuous FM QPT and consequently QCP in "clean" (stoichiometric) systems from the class (2), where the continuous QPT is driven by magnetic field or pressure. The number of such systems is, however, very small [10], because clean systems generically show a discontinuous QPT. The candidate systems are UIr [47], $UNiSi_2$ [48], $U_4Ru_7Ge_6$ [49], and $CeRh_6Ge_4$ [50–52] where in all cases, the QPT is driven by pressure.

There emerges a question whether the intermediate state in the $FeGa_{3-x}Ge_x$ is an ordinary (canonical) SG state or it also contains quantum Griffiths effects? As already discussed, the two necessary ingredients of a canonical SG state are randomness and frustration, so that the spins are positioned randomly in the lattice in a magnetically frustrated configuration. The Griffiths phase, on the other hand, is formed on the paramagnetic side of the QPT and involves so-called rare regions, denoting locally FM ordered (unfrustrated) clusters of spins of arbitrary large spatial size that are free of any magnetic defect (vacant spin site) [53–56]. The dynamics of the rare regions is very slow like in a SG [57], because flipping of their giant moments requires a coherent change of the magnetization over a large volume. The formation of rare regions upon the Ge-for-Ga substitution in the $FeGa_{3-x}Ge_x$ would require nonrandom distribution of the moments on the iron periodic sublattice, with some local regions fully filled with the moments, even though the bulk system is globally still in the paramagnetic phase. This is an unlikely situation to happen in the low-doping regime, suggesting that the intermediate phase is a canonical SG phase. At increased doping, the presence of quantum Griffiths effects cannot be ruled out.

A related issue is the question whether the paramagnetic → SG → FM transition in the $FeGa_{3-x}Ge_x$ fulfills the requirements to be classified as a QPT, or it is still a conventional, thermodynamic phase transition, despite that it happens at such low temperatures? Thermodynamic phase transitions are assisted by thermal fluctuations, while QPTs that occur at

absolute zero are assisted by zero-point quantum fluctuations associated with Heisenberg's uncertainty principle. Thermal fluctuations are temperature-dependent (related to the thermal energy k_BT), whereas quantum fluctuations are temperature-independent, implying that the experimentally observable physical quantities should not depend on the temperature. The Cole-Cole analysis of the ac susceptibility in the QPT region of the $FeGa_{3-x}Ge_x$ has revealed that the slowing-down spin dynamics in the SG state upon cooling remains thermally activated down to the lowest investigated temperature of 0.4 K, indicating that the phase transition is driven by thermal fluctuations at least down to that temperature and is hence thermodynamic in nature. The regime of quantum fluctuations is obviously not yet entered even at 0.4 K.

V. EXPERIMENTAL SECTION

Magnetic measurements were conducted on a Quantum Design MPMS3 magnetometer, equipped with a 7 T magnet and operating at temperatures between 1.8 and 400 K. Lower temperatures down to 0.4 K were reached by iQuantum He3 refrigerator. Since most of the measurements were conducted in low external magnetic fields 0.01–25 mT, the Ultra-Low Field (ULF) option was used to compensate for the residual magnetic field of the superconducting magnet. The low-field experiments were conducted using a copper AC/ULF coil of the MPMS3 magnetometer to ensure an accurate and repeatable magnetic field.

Electrical resistivity and specific heat measurements were performed on a Quantum Design Physical Property Measurement System PPMS 9T, equipped with a 9 T magnet and a He3 refrigerator to reach the temperature of 0.35 K.

ACKNOWLEDGMENT

The Slovenian authors acknowledge the financial support from the Slovenian Research and Innovation Agency (Research Core Funding No. P1-0125 and Project No. N1-0330).

DATA AVAILABILITY

The data that support the findings of this article are not publicly available upon publication because it is not technically feasible and/or the cost of preparing, depositing, and hosting the data would be prohibitive within the terms of this research project. The data are available from the authors upon reasonable request.

APPENDIX: A

Within the Havriliak-Negami relaxation model, the real and imaginary parts of the ac susceptibility, $\chi'(\omega)$ and $\chi''(\omega)$, are given by the expressions [27,28]

$$\chi'(\omega) = \chi_\infty + (\chi_s - \chi_\infty) \times \frac{\cos(\beta\phi)}{[1 + 2(\omega\tau)^\alpha \cos(\pi\alpha/2) + (\omega\tau)^{2\alpha}]^{\beta/2}}, \quad \text{(A1)}$$

$$\chi''(\omega) = (\chi_s - \chi_\infty) \frac{\sin(\beta\phi)}{[1 + 2(\omega\tau)^\alpha \cos(\pi\alpha/2) + (\omega\tau)^{2\alpha}]^{\beta/2}}, \quad \text{(A2)}$$

where

$$\phi = \arctan\left[\frac{(\omega\tau)^\alpha \sin(\pi\alpha/2)}{1 + (\omega\tau)^\alpha \cos(\pi\alpha/2)}\right]. \quad \text{(A3)}$$

The angle $\boldsymbol{\theta}$ in the expression for the distribution function ($\boldsymbol{ln\tau}$), given by Eq. (3) of the main paper is defined as [29]

$$\theta = \arctan\left(\frac{\sin(\pi\alpha)}{(\tau/\tau_0)^\alpha + \cos(\pi\alpha)}\right), \quad \text{(A4)}$$

if the argument of the arctangent is positive, else

$$\theta = \arctan\left(\frac{\sin(\pi\alpha)}{(\tau/\tau_0)^\alpha + \cos(\pi\alpha)}\right) + \pi. \quad \text{(A5)}$$

APPENDIX: B

Graphical presentation of the temperature-dependent χ_s fit parameter, used in the theoretical Cole-Cole fits of the ac susceptibility presented in Fig. 7(b) for the $x = 0.16$ compound, is shown in Fig. 13.

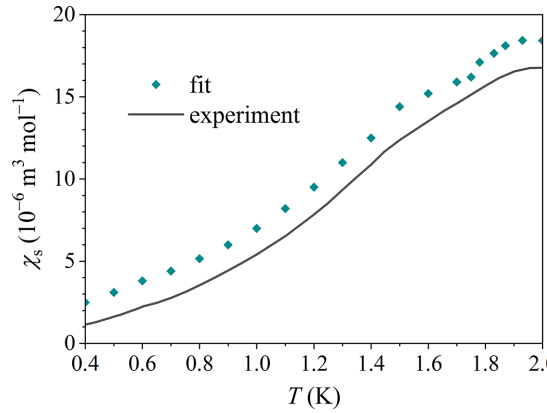

FIG. 13. Temperature dependence of the χ_s fit parameter (green diamonds), used in the theoretical Cole-Cole fits of the ac susceptibility presented in Fig. 7(b) for the $x = 0.16$ compound (the amplitude of the ac field was 0.2 mT and it was applied along the [001] crystallographic direction). Solid curve represents the experimental dc zfc susceptibility of the same compound, with the static field of magnitude 0.2 mT applied along the same direction.

[1] S. Sachdev, *Quantum Phase Transitions* (Cambridge University Press, Cambridge, 1999).

[2] *Understanding Quantum Phase Transitions*, edited by L. D. Carr (CRC Press, Boca Raton, 2010).

[3] M. Vojta, Quantum phase transitions, Rep. Prog. Phys. **66**, 2069 (2003).

[4] P. Coleman and A. J. Schofield, Quantum criticality, Nature (London) **433**, 226 (2005).

[5] S. Sachdev and B. Keimer, Quantum criticality, Phys. Today **64** (2), 29 (2011).

[6] T. Park, F. Ronning, H. Q. Yuan, M. B. Salamon, R. Movshovich, J. L. Sarrao, and J. D. Thompson, Hidden

magnetism and quantum criticality in the heavy fermion superconductor $CeRhIn_5$, Nature (London) **440**, 65 (2006).

[7] H. von Löhneysen, A. Rosch, M. Vojta, and P. Wölfle, Fermi-liquid instabilities at magnetic quantum phase transitions, Rev. Mod. Phys. **79**, 1015 (2007).

[8] P. Gegenwart, Q. Si, and F. Steglich, Quantum criticality in heavy-fermion metals, Nat. Phys. **4**, 186 (2008).

[9] S. Vrtnik, M. Krnel, P. Koželj, Z. Jagličić, L. Kelhar, A. Meden, M.-C. de Weerd, P. Boulet, J. Ledieu, V. Fournée, J.-M. Dubois, and J. Dolinšek, Anisotropic quantum critical point in the Ce_3Al system with a large magnetic anisotropy, J. Phys. Commun. **4**, 105016 (2020).

[10] M. Brando, D. Belitz, F. M. Grosche, and T. R. Kirkpatrick, Metallic quantum ferromagnets, Rev. Mod. Phys. **88**, 039901 (2016).

[11] M. Majumder, M. Wagner-Reetz, R. Cardoso-Gil, P. Gille, F. Steglich, Y. Grin, and M. Baenitz, Towards ferromagnetic quantum criticality in $FeGa_{3-x}Ge_x$: ^{71}Ga NQR as a zero-field microscopic probe, Phys. Rev. B **93**, 064410 (2016).

[12] B. Koo, K. Bader, U. Burkhardt, M. Baenitz, P. Gille, and J. Sichelschmidt, Spin dynamics of $FeGa_{3-x}Ge_x$ studied by electron spin resonance, J. Phys.: Condens. Matter **30**, 045601 (2018).

[13] Y. Kishimoto, D. Kasinathan, H. Yasuoka, K. Bader, P. Gille, U. Burkhardt, and M. Baenitz, Site selective substitution and charge differentiation around Ge atom in $FeGa_{3-x}Ge_x$ proved by Ga-NQR with super-cell calculation, J. Phys. Soc. Jpn. **89**, 083701 (2020).

[14] J. C. Alvarez-Quiceno, M. Cabrera-Baez, R. A. Ribeiro, M. A. Avila, G. M. Dalpian, and J. M. Osorio-Guillén, Emergence of competing magnetic interactions induced by Ge doping in the semiconductor $FeGa_3$, Phys. Rev. B **94**, 014432 (2016).

[15] K. Umeo, Y. Hadano, S. Narazu, T. Onimaru, M. A. Avila, and T. Takabatake, Ferromagnetic instability in a doped band gap semiconductor $FeGa_3$, Phys. Rev. B **86**, 144421 (2012).

[16] A. Takeuchi and A. Inoue, Classification of bulk metallic glasses by atomic size difference, heat of mixing and period of constituent element and its application to characterization of the main alloying element, Mater. Trans. **46**, 2817 (2005).

[17] K. Bader and P. Gille, Single crystal growth of $FeGa_3$ and $FeGa_{3-x}Ge_x$ from high-temperature solution using the Czochralski method, Cryst. Res. Technol. **55**, 1900067 (2019).

[18] U. Häussermann, M. Boström, P. Viklund, Ö. Rapp, and T. Björnägen, $FeGa_3$ and $RuGa_3$: Semiconducting intermetallic compounds, J. Solid State Chem. **165**, 94 (2002).

[19] Y. Hadano, S. Narazu, M. A. Avila, T. Onimaru, and T. Takabatake, Thermoelectric and magnetic properties of a narrow-gap semiconductor $FeGa_3$, J. Phys. Soc. Jpn. **78**, 013702 (2009).

[20] N. Tsujii, H. Yamaoka, M. Matsunami, R. Eguchi, Y. Ishida, Y. Senba, H. Ohashi, S. Shin, T. Furubayashi, H. Abe, and H. Kitazawa, Observation of energy gap in $FeGa_3$, J. Phys. Soc. Jpn. **77**, 024705 (2008).

[21] G. A. Bain and J. F. Berry, Diamagnetic corrections and Pascal's constants, J. Chem. Educ. **85**, 532 (2008).

[22] M. Wagner-Reetz, D. Kasinathan, W. Schnelle, R. Cardoso-Gil, H. Rosner, and Y. Grin, Phonon-drag effect in $FeGa_3$, Phys. Rev. B **90**, 195206 (2014).

[23] Y. Imai and A. Watanabe, Electronic structures of semiconducting $FeGa_3$, $RuGa_3$, $OsGa_3$, and $RuIn_3$ with the $CoGa_3$- or the $FeGa_3$-type structure, Intermetallics **14**, 722 (2006).

[24] J. M. D. Coey, *Magnetism and Magnetic Materials* (Cambridge University Press, Cambridge, 2010), pp. 171–172.

[25] M. Hagiwara, Cole–Cole plot analysis of the spin-glass system $NiC_2O_4 \cdot 2(2MIz)_{0.49}(H_2O)_{0.51}$, J. Magn. Magn. Mater. **177**, 89 (1998).

[26] O. Petracic, S. Sahoo, Ch. Binek, W. Kleemann, J. B. Sousa, S. Cardoso, and P. P. Freitas, Cole–Cole analysis of the superspin glass system $Co_{80}Fe_{20}/Al_2O_3$, Ph. Transit. **76**, 367 (2003).

[27] S. Havriliak and S. Negami, A complex plane analysis of α-dispersions in some polymer systems, J. Polym. Sci. C **14**, 99 (1966).

[28] S. Havriliak and S. Negami, A complex plane representation of dielectric and mechanical relaxation processes in some polymers, Polymer **8**, 161 (1967).

[29] R. Zorn, Applicability of distribution functions for the Havriliak–Negami spectral function, J. Polym. Sci. B **37**, 1043 (1999).

[30] K. C. Kao, *Dielectric Phenomena in Solids* (Elsevier Academic Press, London, 2004), pp. 92–93.

[31] U. Mizutani, *Introduction to the Electron Theory of Metals* (Cambridge University Press, Cambridge, 2001), p. 39.

[32] A. Tari, *The Specific Heat of Matter at Low Temperatures* (Imperial College Press, London, 2003), pp. 167–174.

[33] J. A. Mydosh, *Spin Glasses: An Experimental Introduction* (Taylor & Francis, London, 1993), p. 7 and p. 31.

[34] F. R. Wagner, R. Cardoso-Gil, B. Boucher, M. Wagner-Reetz, J. Sichelschmidt, P. Gille, M. Baenitz, and Y. Grin, On Fe–Fe dumbbells in the ideal and real structures of $FeGa_3$, Inorg. Chem. **57**, 12908 (2018).

[35] K. Binder and A. P. Young, Spin glasses: Experimental facts, theoretical concepts, and open questions, Rev. Mod. Phys. **58**, 801 (1986).

[36] T. R. Kirkpatrick and D. Belitz, Ferromagnetic quantum critical point in noncentrosymmetric systems, Phys. Rev. Lett. **124**, 147201 (2020).

[37] A. Steppke, R. Küchler, S. Lausberg, E. Lengyel, L. Steinke, R. Borth, T. Lühmann, C. Krellner, M. Nicklas, C. Geibel, F. Steglich, and M. Brando, Ferromagnetic quantum critical point in the heavy-fermion metal $YbNi_4(P_{1-x}As_x)_2$, Science **339**, 933 (2013).

[38] M. Nicklas, M. Brando, G. Knebel, F. Mayr, W. Trinkl, and A. Loidl, Non-Fermi-liquid behavior at a ferromagnetic quantum critical point in Ni_xPd_{1-x}, Phys. Rev. Lett. **82**, 4268 (1999).

[39] M. Nicklas, Nicht-Fermi-Flüssigkeitsverhalten am quantenkritischen Punkt in Nickel-Palladium. Ph.D. thesis, University of Augsburg, Germany, 2000.

[40] M. Sato, Magnetic properties and electrical resistivity of $(Ni_{1-x}Pd_x)_3Al$, J. Phys. Soc. Jpn. **39**, 98 (1975).

[41] J. Yang, B. Chen, H. Ohta, C. Michioka, K. Yoshimura, H. Wang, and M. Fang, Spin fluctuations on the verge of a ferromagnetic quantum phase transition in $Ni_3Al_{1-x}Ga_x$, Phys. Rev. B **83**, 134433 (2011).

[42] L. Schoop, M. Hirschberger, J. Tao, C. Felser, N. P. Ong, and R. J. Cava, Paramagnetic to ferromagnetic phase transition in lightly Fe-doped Cr_2B, Phys. Rev. B **89**, 224417 (2014).

[43] D. A. Sokolov, M. C. Aronson, W. Gannon, and Z. Fisk, Critical phenomena and the quantum critical point of ferromagnetic $Zr_{1-x}Nb_xZn_2$, Phys. Rev. Lett. **96**, 116404 (2006).

[44] S. Jia, P. Jiramongkolchai, M. R. Suchomel, B. H. Toby, J. G. Checkelsky, N. P. Ong, and R. J. Cava, Ferromagnetic quantum critical point induced by dimer-breaking in $SrCo_2(Ge_{1-x}P_x)_2$, Nat. Phys. **7**, 207 (2011).

[45] J. A. Mydosh and P. M. Oppeneer, *Colloquium*: Hidden order, superconductivity, and magnetism: The unsolved case of URu_2Si_2, Rev. Mod. Phys. **83**, 1301 (2013).

[46] N. P. Butch and M. B. Maple, The suppression of hidden order and the onset of ferromagnetism in URu_2Si_2 via Re substitution, J. Phys.: Condens. Matter **22**, 164204 (2010).

[47] T. C. Kobayashi, S. Fukushima, H. Hidaka, H. Kotegawa, T. Akazawa, E. Yamamoto, Y. Haga, R. Settai, and Y. Onuki, Pressure-induced superconductivity in ferromagnet UIr without inversion symmetry, Physica B **378**, 355 (2006).

[48] V. A. Sidorov, P. H. Tobash, C. Wang, B. L. Scott, T. Park, E. D. Bauer, F. Ronning, J. D. Thompson, and Z. Fisk, Quenching of ferromagnetism in $\beta - UB_2C$ and $UNiSi_2$ at high pressure, J. Phys.: Conf. Series **273**, 012014 (2011).

[49] H. Hidaka, S. Takahashi, Y. Shimizu, T. Yanagisawa, and H. Amitsuka, Pressure-induced quantum critical point in ferromagnet $U_4Ru_7Ge_6$, J. Phys. Soc. Jpn. **80**, SA102 (2011).

[50] H. Kotegawa, E. Matsuoka, T. Uga, M. Takemura, M. Manago, N. Chikuchi, H. Sugawara, H. Tou, and H. Harima, Indication of ferromagnetic quantum critical point in Kondo lattice $CeRh_6Ge_4$, J. Phys. Soc. Jpn. **88**, 093702 (2019).

[51] B. Shen, Y. Zhang, Y. Komijani, M. Nicklas, R. Borth, A. Wang, Y. Chen, Z. Nie, R. Li, X. Lu, H. Lee, M. Smidman, F. Steglich, P. Coleman, and H. Yuan, Strange-metal behaviour in a pure ferromagnetic Kondo lattice, Nature (London) **579**, 51 (2020).

[52] Y. J. Zhang, Z. Y. Nie, R. Li, Y. C. Li, D. L. Yang, B. Shen, Y. Chen, F. Du, S. S. Luo, H. Su, R. Shi, S. Y. Wang, M. Nicklas, F. Steglich, M. Smidman, and H. Q. Yuan, Suppression of ferromagnetism and influence of disorder in silicon-substituted $CeRh_6Ge_4$, Phys. Rev. B **106**, 054409 (2022).

[53] R. B. Griffiths, Nonanalytic behavior above the critical point in a random Ising ferromagnet, Phys. Rev. Lett. **23**, 17 (1969).

[54] A. J. Bray, Nature of the Griffiths phase, Phys. Rev. Lett. **59**, 586 (1987).

[55] A. J. Millis, D. K. Morr, and J. Schmalian, Quantum Griffiths effects in metallic systems, Phys. Rev. B **66**, 174433 (2002).

[56] T. Vojta, Quantum Griffiths effects and smeared phase transitions in metals: Theory and experiment, J. Low Temp. Phys. **161**, 299 (2010).

[57] M. Randeria, J. P. Sethna, and R. G. Palmer, Low-frequency relaxation in Ising spin-glasses, Phys. Rev. Lett. **54**, 1321 (1985).